Journal of Population Therapeutics & Clinical Pharmacology

RESEARCH ARTICLE
DOI: 10.53555/kqp0mj79

INVESTIGATION OF THERMODYNAMIC MODELS AND HEAT TRANSFER DURING LASER RADIATION IN TEETH TISSUE

Bita Aramesh[1*]

[1*]Specialist in surgery and root canal treatment (Endodontist), University of Sistan and Baluchistan, Zahedan, Iran dr.aramesh20@yahoo.com

***Corresponding author:** Bita Aramesh
*Specialist in surgery and root canal treatment (Endodontist), University of Sistan and Baluchistan, Zahedan, Iran dr.aramesh20@yahoo.com

Abstract
In this study, the thermal behavior of human teeth under laser irradiation is investigated. Due to the high power and short duration of laser exposure, deviations from the Fourier heat transfer model can occur. To address this limitation, the Dual-Phase-Lag (DPL) non-Fourier heat transfer model is employed. The study focuses on a two-rooted wisdom tooth, where the DPL model equations are solved using the finite volume method to obtain the thermal response of the tooth under laser exposure. The effects of the phase lags, which are parameters of the DPL model and cause deviations from the Fourier model, are thoroughly analyzed in relation to the thermal behavior of the tooth. The results indicate that the non-Fourier model can produce a significantly different temperature distribution compared to the Fourier model. The extent of this deviation is determined by the two phase lags in the DPL model. To determine the optimal phase lags, inverse heat transfer methods were utilized. By applying the Levenberg-Marquardt method and utilizing experimental data from previous studies, the optimal phase lags were identified, demonstrating that the non-Fourier model is more suitable for simulating laser irradiation on teeth compared to the Fourier model. For instance, in the case of laser irradiation delivering 28,000 joules per square meter over 5 seconds, the Fourier model predicts a maximum temperature difference of approximately 40°C, whereas experimental results report a difference of around 22°C. Assuming the tooth behaves as a non-Fourier material with parameters $\tau_t = 3$ and $\tau_p = 3$, the calculated temperature difference is approximately 25°C, which closely aligns with the experimental findings.

Key words:
human tooth, laser radiation, finite volume method, heat transfer, thermodynamics, Fourier, non-Fourier,

1. Introduction

Endodontic treatment is the standard of care for teeth with pulp and/or periapical lesions, aiming to restore functionality within the entire dento-maxillary apparatus and improve the patient's quality of life [1]. The success of this treatment largely hinges on the thorough elimination of bacteria and the smear layer within the root canals [2,3]. Traditionally, root canal preparation involves irrigation with various bactericidal solutions, such as sodium hypochlorite and EDTA, which require direct contact with the dentine surface. Modern approaches to mechanical root canal instrumentation include the use of endodontic files with a large taper, which come with certain risks, including perforations and

stripping. These techniques, while less conservative in preparing the root canal walls, can reduce the mechanical strength of the root walls, potentially compromising future tooth restoration. Nonetheless, they are effective in removing debris and enhancing the access of irrigants, thereby improving the disinfection of the endodontic system [4,5,6,7]. Sodium hypochlorite remains the most widely used solution for irrigating root canals due to its ability to dissolve organic matter and effectively eradicate microorganisms. The best outcomes are achieved with higher concentrations of hypochlorite solution (4% or 5.25%). EDTA is also employed alongside sodium hypochlorite to remove the smear layer from the root canal. The efficacy of these solutions can be enhanced through agitation by sonic or ultrasonic activation [8,9]. Given the limited penetration of these irrigants into the dentinal canals—up to a maximum of 100 μm—while bacteria can be present as deep as 1000 μm [10], and recognizing that root canal instrumentation cannot reach all ramifications of the endodontic system, it is essential to incorporate a root canal decontamination technique into the endodontic treatment protocol to prevent the development of recurrent infections [8]. A contemporary method for reducing the bacterial load in the root canal involves the use of dental lasers for irradiation [2].

A laser functions as a light amplifier, enhancing specific properties of light energy. Most devices used in low-level or low-intensity laser therapy emit light within the red visible and near-infrared regions of the electromagnetic spectrum, with typical wavelengths ranging from 600 to 1000 nm. These devices typically have low mean power values, between 1 and 100 mW, though their maximum power output can exceed 100 mW. Today, advanced laser-based equipment, such as that used for root canal therapy, is widely employed in dentistry [4], [5]. However, this technique carries the risk of causing damage to the pulp or the enamel and dentin layers [6]. While the enamel and dentin are solid tissues, the dental pulp is a soft tissue containing nerves [7]. The potential for laser-induced thermal damage to the pulp raises concerns about the intensity of the laser used. Numerous studies have confirmed the effectiveness of these medical devices. Falahatkar et al [10], Evaluation of heat conduction in a laser irradiated tooth with the three-phase-lag bio-heat transfer model. Sabaeian et al. [11] explored the potential use of lasers for the removal of dental caries. Chiang et al. [12] investigated various types of lasers, including CO2, ER, and ND, for their applications in dental equipment. Laser usage in dentistry involves the science of thermal processes at a micro scale and operates with minimal radiation time. Lau et al [13], They investigated the heat generated during dental treatments that affects the temperature inside the pulp. Wight et al [14]. conducted studies on the thermal conductivity of thin layers. Wang et al [15], Numerical analysis and experimental verification of time-dependent heat transfer under ultrashort pulse laser are discussed. Petersen et al [16] They evaluated the thermal effects on the dental pulp during the bleaching process with the help of a diode laser. Deppe et al [17] In their study, they investigated the thermal effect of 445 nm diode laser on five dental implant systems: a laboratory study.

In laser dentistry applications, precise temperature control at various points within the tooth is crucial to prevent damage to sensitive tissues [18]. Therefore, the use of non-Fourier heat transfer models, which account for the limitations in heat transfer speed, is deemed necessary [19]. The Fourier model is widely utilized for analyzing thermal problems, but in many real-world scenarios, this model fails to accurately predict the actual behavior of thermal systems. This shortcoming is particularly evident in situations involving rapid temperature changes and high heat fluxes [20]. One such scenario is laser irradiation of a tooth, where heat is suddenly applied to the tooth on a very small scale [21]. During laser irradiation, heat is transferred to the tooth with high intensity over a short period. Under such conditions, deviations from the Fourier model become significantly noticeable, necessitating the use of non-Fourier models capable of accounting for the limited speed of heat transfer [22]. Non-Fourier models, such as the dual-phase-lag (DPL) bio-thermal model, can predict temperature variations with greater accuracy. These models are able to more precisely evaluate the effects of heat transfer delay and the thermal impacts resulting from concentrated heat sources [23].

In this study, a non-Fourier heat transfer model with dual-phase lag (DPL) has been presented to investigate the thermal behavior of human teeth under laser irradiation. While previous research has predominantly relied on Fourier heat transfer models or simpler approaches, this study specifically examines the potential deviations from the Fourier model in scenarios involving high-power, short-

duration laser irradiation. The innovation of this research lies in applying the DPL model to analyze the thermal behavior of teeth and utilizing inverse heat transfer methods to determine the optimal phase lag times. The findings of this study indicate that the non-Fourier model provides more accurate predictions of temperature distribution and final temperature differences in teeth under laser irradiation, aligning more closely with experimental results than Fourier models. The exploration of non-Fourier models in laser irradiation scenarios can contribute to the improvement of laser device design and cooling systems in dentistry. This research has the potential to lead to the development of new standards and enhanced treatment processes, ultimately improving treatment quality and patient satisfaction. Furthermore, in scientific and engineering fields, a better understanding of thermal behavior under specific conditions can result in significant advancements in the design of new materials and advanced technologies. A thorough examination of these models and their comparison with classical models could foster the creation of innovative and more efficient methods for analyzing and controlling thermal processes across various industries and scientific applications.

2. Research Methodology

The relationship between heat flux and temperature gradient, known as the constitutive equation, is one of the fundamental principles of heat conduction. The Fourier model, the first heat transfer model, was introduced by Joseph Fourier in 1807 and assumes that the heat transfer speed is infinite [24]. While this model is accurate in many industrial applications, in situations such as high-power laser irradiation where heat is transferred rapidly, it is necessary to account for deviations from the Fourier model. One corrective approach to address this deviation is the dual-phase-lag (DPL) bio-heat model, which assumes that changes in temperature and heat flux occur at a finite speed [25].

2.1. Dual-Phase-Lag (DPL) Bio-Heat Method

The Fourier heat transfer equation for a body in general is in the form of equation (1):

$$\rho c \frac{\partial \tau}{\partial \tau} = k\nabla^2 T + q \quad (1)$$

In nature, under certain conditions such as the application of high heat flux in a short period or within living organisms, the thermal behavior of materials does not follow the Fourier equation. This deviation is due to the finite speed of heat transfer.

To account for this behavior, a relaxation time is considered for the conversion of heat into a temperature difference, and hyperbolic temperature-wave equations replace the Fourier equation. In these equations, the Fourier equation is replaced by a modified relationship as follows [26]:

$$q(r,t) + \tau_q \frac{\partial q(r,t)}{\partial r} = -k\nabla T(r,t) \qquad (2)$$

If the left side of the hyperbolic temperature wave equation is expanded by Taylor's first order amplification:

$$q\left(r, t + \tau_q\right) = -k\nabla T(r,t) \qquad (3)$$

The latter equation states that there is a delay between the heat given to the object and the resulting temperature gradient. Considering the energy conservation equation without having an energy source:

$$\rho c \frac{\partial \tau}{\partial \tau} = \nabla . q \qquad (4)$$

By combining equation (3) and energy conservation equation (4):

$$\tau_q \frac{\partial (\rho c \frac{\partial \tau}{\partial \tau})}{\partial r} + \rho c \frac{\partial \tau}{\partial \tau} = \nabla . \left(k\nabla T(r,t)\right) \qquad (5)$$

Recently, Antaki [27] used the conduction heat transfer equation with two delay phases. This model is based on the concept of two-phase delay. The second delay enters the equations as follows:

$$q(r,t+\tau_q) = -k\nabla T(r,t+\tau_t) \qquad (6)$$

where τ_t is the delay time for the temperature gradient, if the above equation is expanded with the first degree Taylor approximation:

$$q(r,t) + \tau_q \frac{\partial q(r,t)}{\partial r} = -k\left(\nabla T(r,t) + \ \tau_T \frac{\partial \nabla T(r,t)}{\partial t}\right) \qquad (7)$$

If equation (2) and (7) are combined, the conduction heat transfer equation with two delay phases is obtained. For axially symmetric geometry, the above equation is as follows [8]:

$$\tau_q \frac{\partial^2 T}{\partial t^2} + \frac{\partial T}{\partial t} = \alpha\left(\frac{1}{r}\frac{\partial}{\partial r}\left(r\frac{\partial T}{\partial r}\right) + \frac{\partial^2 T}{\partial z^2}\right) + \ \tau_t \frac{\partial}{\partial t}\left(\alpha\ \frac{1}{r}\frac{\partial}{\partial r}\left(r\frac{\partial T}{\partial r}\right) + \frac{\partial^2 T}{\partial z^2}\right) \qquad (8)$$

2.2. Geometry Under Investigation

Figure (1) schematically illustrates a semi-sectioned two-rooted tooth. To develop the final model, the profile of a wisdom tooth with two roots was used as a sample. A two-dimensional model of the tooth geometry was first created, and then by rotating it around the vertical axis, a three-dimensional geometry of the two-rooted tooth was constructed. The tooth root is symmetric with respect to its axis, and the tooth crown is also symmetrically positioned around the axis. This geometry provides a very good approximation for solving the heat transfer equation in the tooth and analyzing its temperature. However, if parameters such as stress were under investigation, this approximation would be insufficient, and a more accurate representation of the tooth's geometry would be necessary.

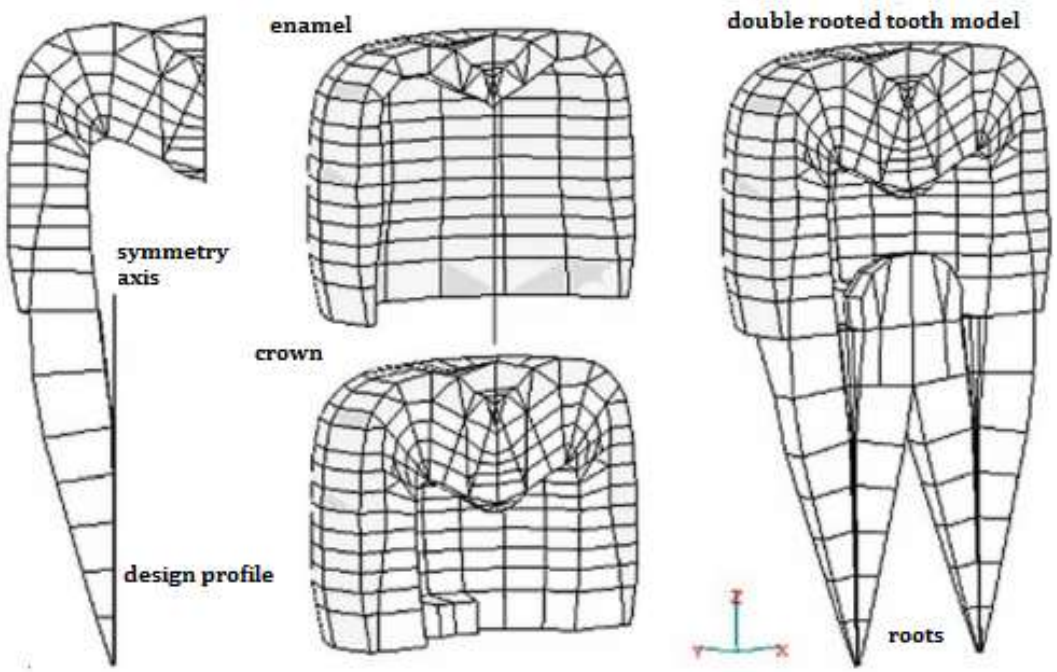

Figure 1. A view of the investigated geometry

The tooth geometry consists of two main sections: enamel (the hard, outer layer) and dentin (the internal layer). The dimensions of the tooth are based on actual size, with a volume of 0.6 cubic meters and a mass of 1.47 grams. This geometry was selected because it aligns with relevant experimental results, allowing for comparison with the data obtained in the present study. The properties of these two sections of the tooth are provided in the table below.

Table 1. Thermal properties of dental components

Physical property	Mina	ivory
Special heat (J/kg.K)	750	1170
Thermal conductivity (W/m.K)	0.92	0.63

density (kg/m3)	2900	2100

2.3. Boundary and Initial Conditions

The appropriate initial conditions are defined as follows:

$$T(r,z,0) = T_0 \qquad (9)$$

$$\frac{\partial T}{\partial t}(r,z,0) = 0 \qquad (10)$$

If the Fourier equation is used to solve the problem, equation (11) is sufficient as an initial condition. It is assumed that the heat flux q_L enters the tooth from the top and in the radius R_L, k_1 represents the conductivity coefficient of tooth enamel.

$$-k_1 \frac{\partial T}{\partial z}(r,0,t) = q_L\,, \qquad 0 \le r \le R_L \text{ و } t \le T_L \qquad (11)$$

R_L is equal to 600 µm exposed to direct radiation. Of course, this equation holds up to time T_L. That is, as long as the laser shines on the tooth and for the times after T_L, the following equation is valid.

$$-k_1 \frac{\partial T}{\partial z}(r,0,t) = 0\,, \qquad 0 \le r \le R_L \text{ و } t \le T_L \qquad (12)$$

The rest of the enamel surfaces are assumed to be in displacement heat transfer with the oral environment.

$$-k_1 \frac{\partial T}{\partial z}(r,0,t) = h\,(T_\infty - T) \qquad enamel\ sur\ free \qquad (13)$$

For the contact surfaces of enamel and dentin, the condition of continuity of temperature and heat flux is considered:

$$-k_1 \frac{\partial T}{\partial z}(r,t) = k_2 \frac{\partial T}{\partial z}(r,t) \qquad interface\ of\ enamel\ sur\ free \qquad (14)$$

$$T(r,t) = T(r,t) \qquad interface\ of\ enamel\ sur\ free \qquad (15)$$

2.4. Discretization of equations

The first derivative is discretized by the central Eulerian method as follows [14].

$$\frac{\partial T}{\partial z} = \frac{T_{i+1} + T_{i-1}}{2 * \Delta t} \qquad (16)$$

For the discretization of the second derivative, Euler discretization, which is the simplest type of discretization, has been used.

$$\frac{\partial T}{\partial z} = \frac{T_{i+1} - T_{i-1} - 2 * T_i}{\Delta t^2} \qquad (17)$$

For discretizing the Laplacian term, a corrected Gauss-Seidel method is used. This method requires values on the faces of the grid cells. Since in the finite volume method, values are considered at the center of the cell volumes, the results need to be interpolated onto the faces of the cells. In the present study, linear interpolation is employed for this purpose.

To discretize the third derivative, which is the most challenging part of the work, the approach of breaking it into two separate Laplacian components is utilized.

$$\frac{\partial \nabla^2 T}{\partial t} = \frac{\nabla^2 T^{(n+1)} - \nabla^2 T^{(n)}}{\Delta t} \qquad (18)$$

This paper examines the deviation of the nonlinear behavior of teeth from the Fourier equation. To accurately determine this deviation, an optimization method combined with experimental data is employed. The Levenberg-Marquardt method, which is commonly used for nonlinear problems, has been applied for this purpose. This method is also applicable in linear problems with poor conditions, where conventional linear algorithms may not perform well.

The Levenberg-Marquardt method is fundamentally designed to solve nonlinear problems, but it is also applicable in linear problems where conventional linear algorithms cannot be used due to unsuitable conditions. The method generally includes the following steps:

1. **Direct Solution:** Initially, the problem is solved directly.
2. **Inverse Solution:** Then, the inverse problem is solved to determine the unknown parameters.

3. **Iterative Process:** Using an iterative process, the results are refined and converge towards the final solution.
4. **Stopping Criterion:** A stopping criterion is set, and the process is halted when this criterion is met.
5. **Computational Algorithm:** A computational algorithm is used to perform the above steps and achieve the final solution.

Transient heat transfer in a wall is considered as shown in Figure 2. This wall is dimensionless, initially at a temperature of zero, and both boundaries at $x = 0$ and $x = 1$ are insulated. Additionally, a heat source $g_p(t)$ releases energy at the location $x = 0.5$.

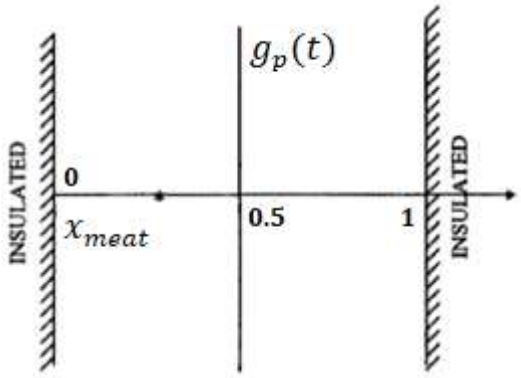

Figure 2. Schematic of transient heat transfer geometry in a wall.

The mathematical formulation of this problem in dimensionless form is given as follows:

$$\frac{\partial^2 T(x,t)}{\partial x^2} + g_p(t)\delta(x-0.5) = \frac{\partial T_{(x,t)}}{\partial t} \qquad t > 0\ , 0 < x < 1 \qquad (20)$$

$$\frac{\partial T(0,t)}{\partial x} = 0 \qquad x = 0\ for\ \ t > 0 \qquad (21)$$

$$\frac{\partial T(0,t)}{\partial x} = 0 \qquad x = 1\ for\ \ t > 0 \qquad (22)$$

$$T(x,0) = 0 \qquad 0 < x < 1\ for\ t = 0 \qquad (23)$$

4.1. Findings

4.1. Validation of the solver

In this section, the solver developed for non-Fourier problems is validated. Given the challenging nature of non-Fourier equations, it is essential to first verify the accuracy of the solver. The validation in this study is carried out using two previous works. The first case involves the analytical solution of the non-Fourier DPL equation in a one-dimensional body. The second case is the numerical solution of a cylindrically symmetric problem. It is demonstrated that in both cases, the results obtained from the developed solver in this research closely match the results from previous studies. Therefore, the solver can be used to address other non-Fourier problems.

4.1.1. Analytical Solution by Tzou

In 1995, Tzou obtained an analytical solution for the one-dimensional case of the non-Fourier DPL model. The equation, along with the boundary and initial conditions solved by him, are presented in Equations (4-1) to (4-5).

$$\tau_q \frac{\partial^2 T}{\partial t^2} + \frac{\partial t}{\partial t} = \left(\frac{\partial^2 T}{\partial z^2}\right) + \tau_T \frac{\partial}{\partial t}\left(\frac{\partial^2 T}{\partial z^2}\right)$$

$$T = 0\ ,\ \ t = 0$$

$$\frac{\partial T}{\partial t} = 0\ \ ,\qquad t = 0$$

$$T = 1 \quad , \quad z = 0$$
$$\frac{\partial T}{\partial z} = 0 \quad , \quad z = 0$$

In the present study, the problems have been solved in three dimensions. To address the current problem, a cubic domain with dimensions of 1 has been considered, with a boundary condition applied along one arbitrary direction, consistent with the established equations. The other boundary conditions have been set to have a zero temperature gradient (i.e., insulated boundaries). In this way, the geometry can be considered as one-dimensional, where temperature variations occur only in one direction. Figure 3, illustrates the temperature variations in this one-dimensional body. These variations are considered under the following three cases:

1) $\tau_q = 0.05$ & $\tau_T = 0$ For continuous blue line.
2) $\tau_q = 0.05$ & $\tau_T = 0.001$ For the section line.
3) Fourier mode as line-point combination.

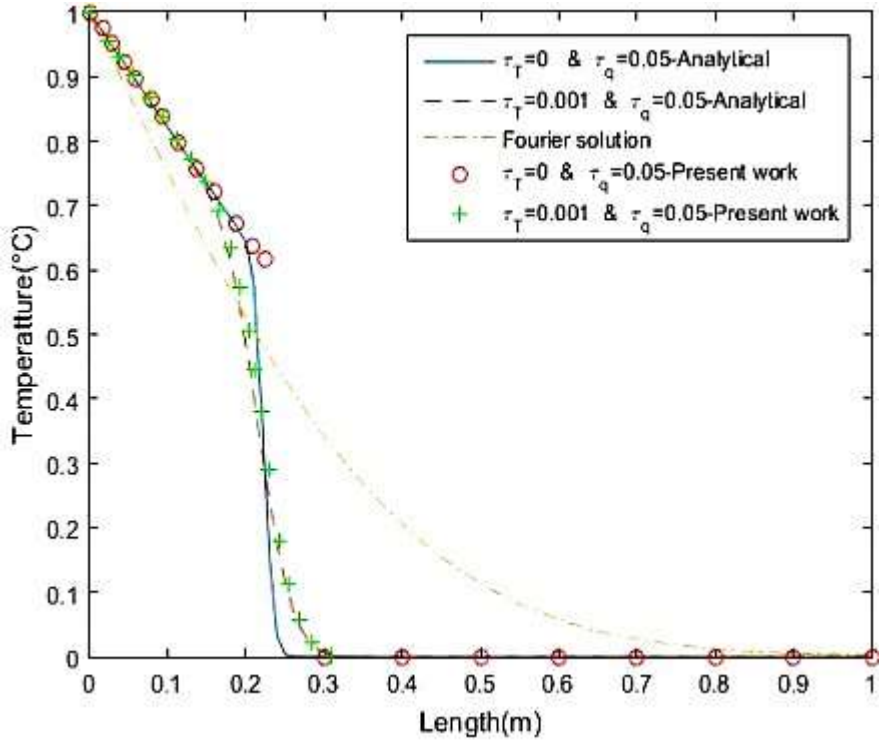

Figure 3. Comparison of the present work with the results of Tezo's analytical solution.

As shown in Figure 3, the developed solver demonstrates a high level of accuracy and closely matches the one-dimensional analytical solution in nearly all cases. Additionally, by closely examining the figure, it can be observed that the non-Fourier case exhibits a lower magnitude and depth of thermal penetration compared to the Fourier case.

4.1.2. Numerical Solution by Zhou

In 2009, Zhou et al [28] solved the non-Fourier DPL equation for an axially symmetric cylinder, as depicted in Figure 4. The corresponding equations and boundary conditions are presented as follows, where the black region represents r_p.

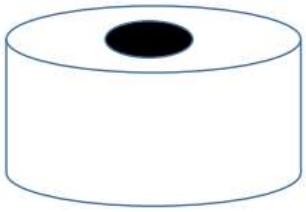

Figure 4. axially symmetric cylinder

The black area in Figure 4, represents the part of the object that is under constant temperature. If this black area is equal to the radius of the object, the result will be similar to the one-dimensional case mentioned in the previous section. The results are examined under the following two conditions.

1) r_p/R=0.05
2) r_p/R=0.5

In Figure 5, the temperature distribution along the cylinder axis is shown for two assumed cases. As illustrated in the figure, the numerical results of the present work and the previous work exhibit nearly identical behavior and are very closely matched. Based on the obtained results, the accuracy of the developed solver can be confirmed, and it can be used for various problems.

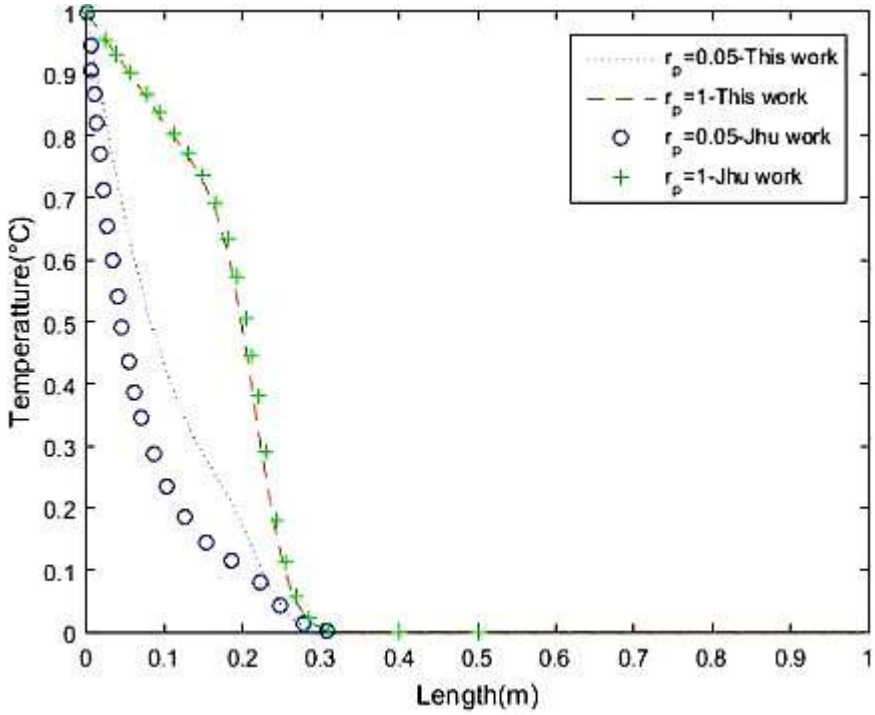

Figure 5. Comparison of the results of the present study with Zhou's numerical solution in 0.05 seconds.

4.2. Independence from Mesh

In simulations, one of the parameters that can influence how closely the results align with the actual solution is the mesh size. To ensure that our results are not dependent on the mesh size, certain steps must be taken to achieve what is known as mesh independence. In transient problems, where the solution is also time-dependent, it is necessary to consider both spatial and temporal grids and demonstrate that the results are independent of the grid types for both parameters. In the next section, mesh independence for both cases will be examined separately.

4.2.1. Independence from the time grid

In this section, the effect of time step has been investigated for several different modes

$$\tau_q = 3 \ \& \ \tau_T = 4$$

In all cases, the conditions have been considered constant. The figure (6) shows the impact of the time step on the solution. It is important to note that the point under investigation is selected on the axis and at the tooth's edge.

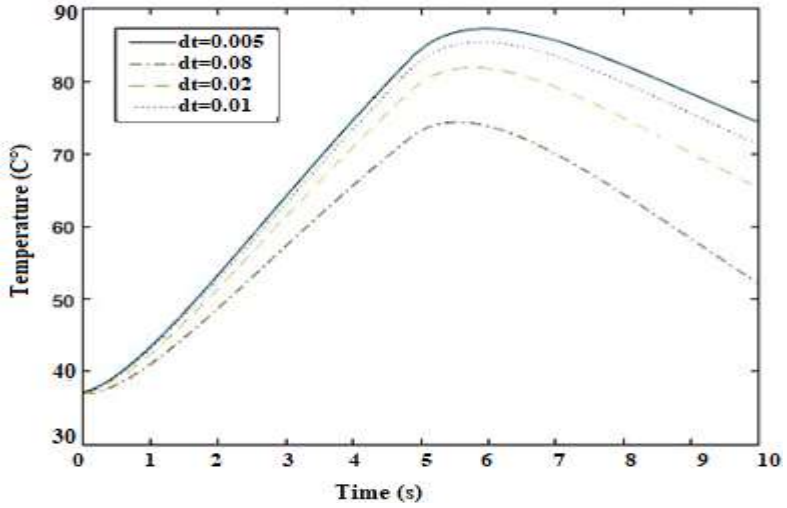

Figure 6. Examining the effect of time step on the answer

As shown in Figure 6, reducing the time step decreases the differences between the solutions, leading to sufficient convergence. Therefore, considering the adequate accuracy and time cost, a time step of 0.01 is chosen for the continuation of the solution. Consequently, in all cases, a time step of 0.01 is assumed unless otherwise stated in the text.

4.2.2. Independence from the network (local)

To assess whether the generated mesh is in an optimal state, the tooth geometry was meshed in four different scenarios. These four cases contain 500 thousand, 750 thousand, one million, and one and a half million mesh cells, respectively. The figure illustrates the effect of mesh count on the solution. For evaluation, points along the axis were selected at the 5-second mark.

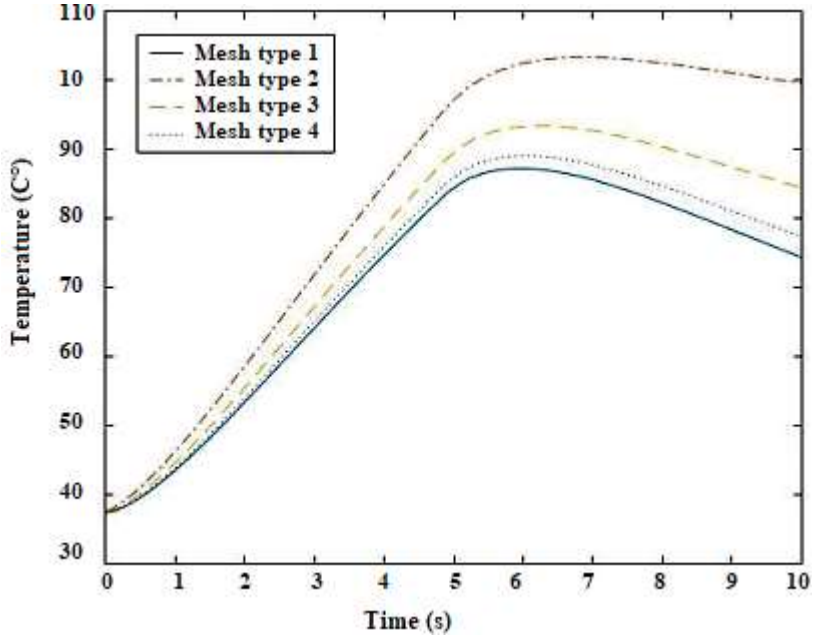

Figure 7. Investigating the effect of the amount of networking on the answer.

Based on Figure 7, it can be observed that the third and fourth mesh types produce nearly identical results. Therefore, it is possible to choose the mesh that requires less runtime. Consequently, the third mesh, containing one million cells, is selected for further calculations and analyses.

4.3. Discussion and Analysis of Various Parameters on Tooth Temperature Distribution
In this section, the temperature distribution of the tooth in different states has been analyzed and plotted using various equations. It should be noted that $q1 = 6.4 J/cm^2$ and $r1$ is assumed to be 600 micrometers. The other properties of the tooth are provided in the table below.

Table 2. Thermal properties of teeth

Physical property	Mina	ivory
Special heat	750	1170
Thermal conductivity	0.92	0.63
density	2900	2100

4.3.1. Analysis of the Parameter τ_q
Figure 8, illustrates the impact of the parameter τ_q on the temperature distribution of the tooth. In this scenario, τ_T is kept constant at 0.5, while τ_q takes values of 0, 0.1, and 5, respectively. This figure demonstrates the temperature distribution along the surface of the tooth and along the axis, where $r = 0$.

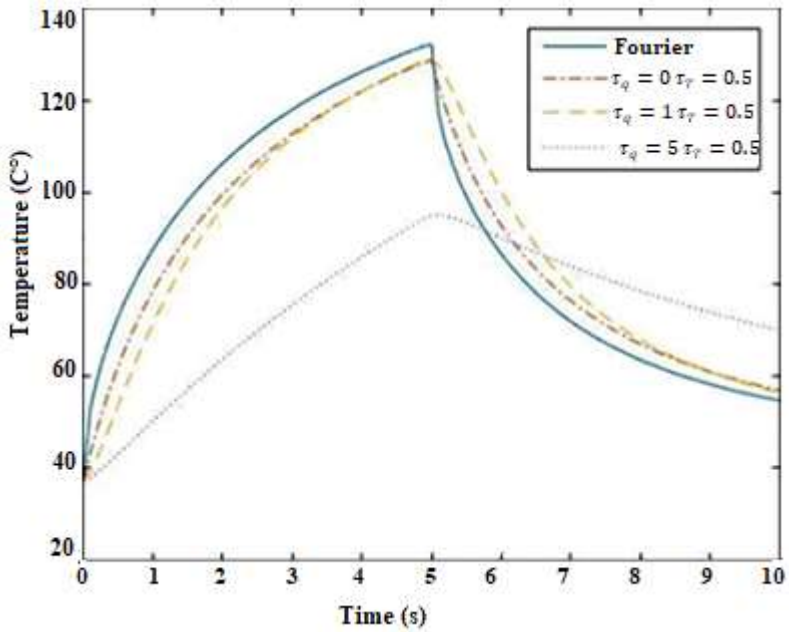

Figure 8. Investigating the τ_q parameter on tooth temperature distribution.

By closely examining Figure 8, the following points can be observed:
1. As the relaxation coefficient τ_q increases in a constant τ_T, the deviation from the Fourier model becomes more pronounced.
2. With an increase in τ_q, the maximum temperature reached within the body decreases.
3. The changes in temperature with variations in τ_q follow a similar and predictable pattern at different heights.
4. When the laser is actively irradiating the body, the Fourier model exhibits a higher temperature compared to the non-Fourier model. However, after the laser's effect ceases and time progresses, the more non-Fourier the model is considered, the higher the temperature will be.

4.3.2. Analysis of the Parameter τ_T

Figure 9, illustrates the effect of the parameter τ_T. In this scenario, τ_T is kept constant at 0.5, while τ_q takes values of 0, 0.1, and 5, respectively. This figure shows the temperature distribution on the surface of the tooth and along the axis where $r = 0$.

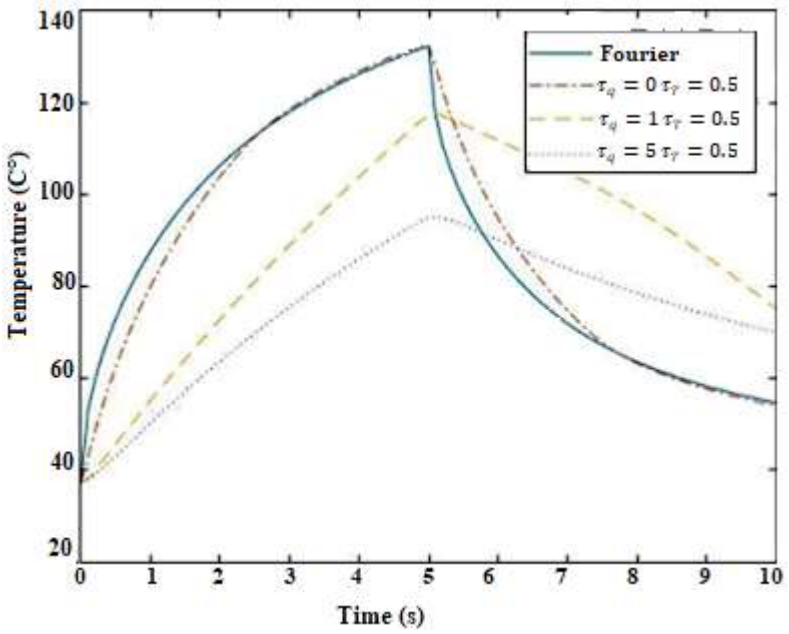

Figure 9. Investigating the τ_T parameter on tooth temperature distribution.

Based on the recent chart, the following conclusions can be drawn:

1. As the relaxation coefficient τ_T increases in a constant τ_q, the deviation from the Fourier model becomes more pronounced.
2. Compared to τ_q, increasing τ_T causes the temperature change curve to become smoother, and the temperature drop in the body after the laser is removed occurs more gradually.
3. With an increase in τ_T, the maximum temperature reached within the body decreases.
4. The changes in temperature with variations in τ_T follow a similar and predictable pattern at different heights.
5. During the times when the laser is irradiating the object, the Fourier mode has a higher temperature than the non-Fourier mode, but with the cessation of the laser effect and the passage of time, the more non-Fourier model is considered, the temperature will be higher.

3.3.3. Checking the temperature on the axis of the tooth at different times

In this section, the temperature distribution on the axis of the tooth is drawn at four different times, so that the effect

To show the non-Fourianity, the temperature distribution in four different states has been investigated in the following order.

Fourier states mean:

1) $\tau_q = 0\ \&\ \tau_T = 0$
2) $\tau_q = 0.5\ \&\ \tau_T = 20$
3) $\tau_q = 20\ \&\ \tau_T = 0.5$
4) $\tau_q = 10\ \&\ \tau_T = 10$

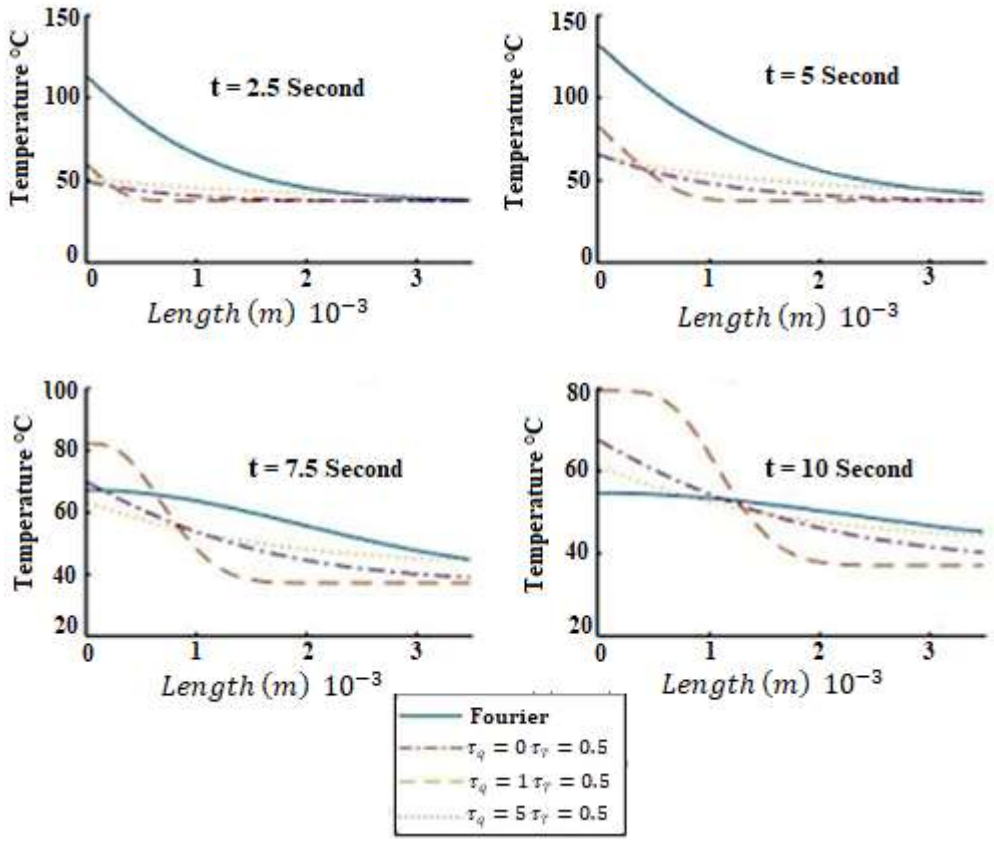

Figure 10. Tooth axis temperature distribution in Fourier and non-Fourier mode.

By examining Figure 10, the following conclusions can be drawn:

1. As the deviation from the Fourier model increases, heat penetrates into the material more slowly.
2. The effect of parameter τ_q is less significant compared to τ_T, in the sense that as τ\tauτ increases, the deviation from the Fourier model increases more rapidly.
3. The maximum temperature of the material decreases with increasing deviation from the Fourier model.
4. As the model deviates further from the Fourier model, the time required for the material to reach thermal equilibrium after the laser radiation is turned off increases.
5. During laser radiation, the temperature of the material in the Fourier model is always higher than in the non-Fourier model (regardless of the factor), but after the laser radiation is turned off, the temperature in the non-Fourier model gradually surpasses that of the Fourier model.

4.3.4. Examination of Tooth Temperature at a Radius of $r = 0.1$ Along the Height

In this section, similar to the previous case, the temperature distribution in various Fourier and non-Fourier states along the radial direction is examined. The difference in this section compared to the previous one is that the radius of the examined points is not assumed to be zero. Instead, the temperature distribution is plotted for a radius of 0.1 in four different cases, as shown in Figure 9-4.
Fourier states mean:

1) $\tau_q = 0$ & $\tau_T = 0$
2) $\tau_q = 0.5$ & $\tau_T = 20$
3) $\tau_q = 20$ & $\tau_T = 0.5$
4) $\tau_q = 10$ & $\tau_T = 10$

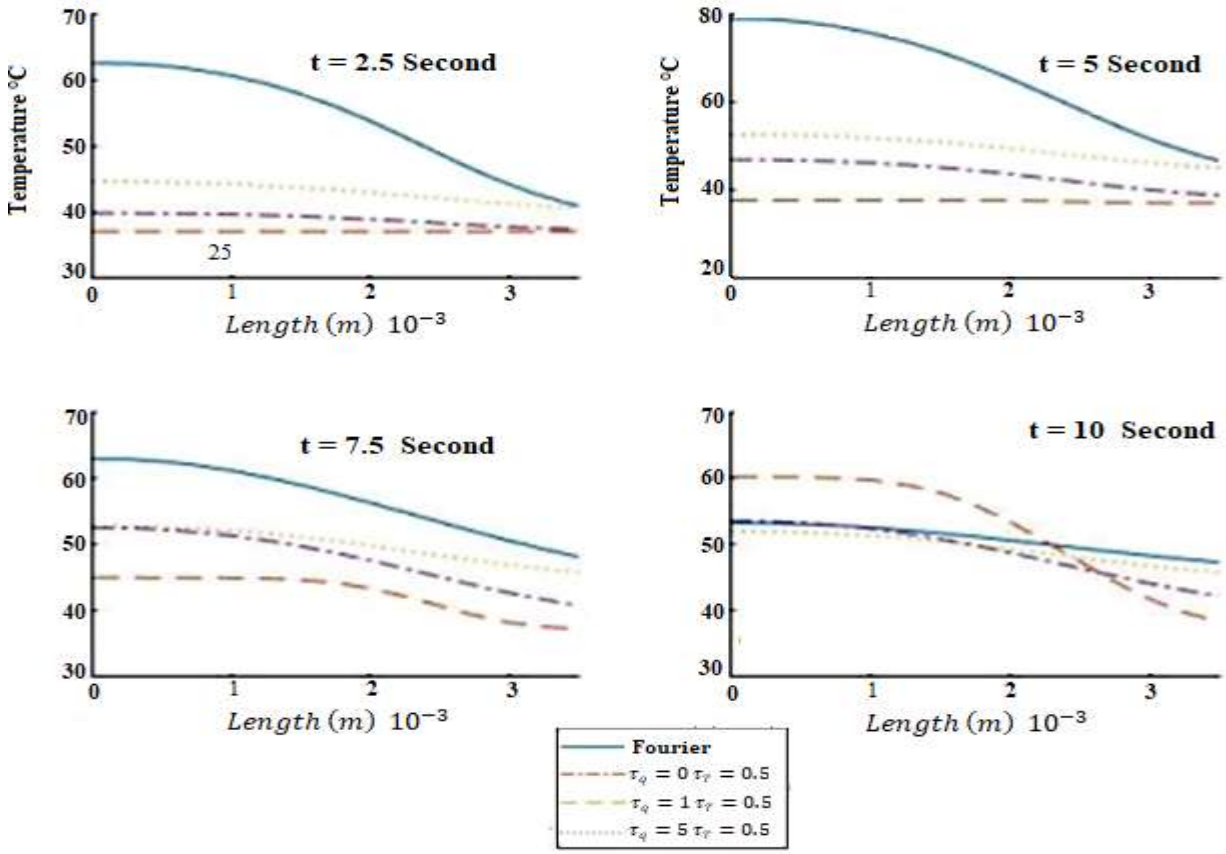

Figure 11. Tooth axial temperature distribution (r=0.1) in Fourier and non-Fourier now.

4.3.5. Radial Temperature Distribution at z = 0.1

In this section, the radial temperature distribution at a height of 0.1 cm below the radiation boundary is examined. To investigate the non-Fourier effects, three non-Fourier curves are plotted in Figure 11.

1) $\tau_q = 0$ & $\tau_T = 0$
2) $\tau_q = 0.5$ & $\tau_T = 20$
3) $\tau_q = 20$ & $\tau_T = 0.5$
4) $\tau_q = 10$ & $\tau_T = 10$

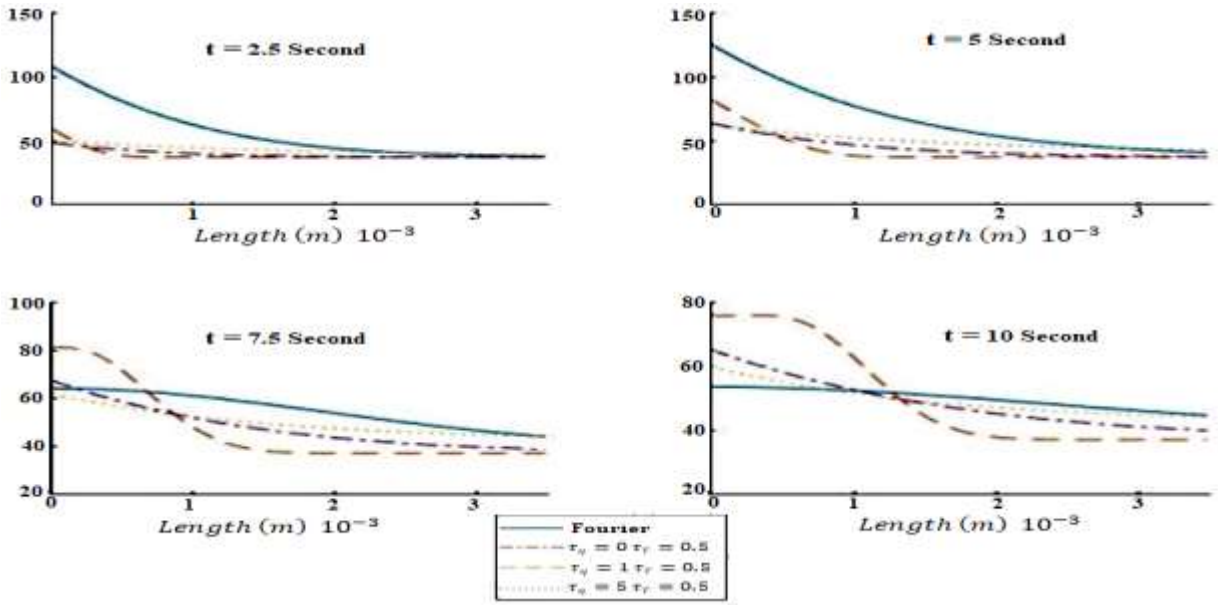

Figure 12. Radial tooth temperature distribution (z=0.1) in Fourier and non-Fourier now.

The results of Figure 12 showed that, In the non-Fourier case, heat penetration into the material occurs with a time delay. This delay is due to the limited heat transfer speed inherent in the non-Fourier model, making this behavior predictable and clearly demonstrating the deviation from the Fourier model. In the Fourier model, as long as the material is exposed to heat transfer, the temperature increases in a larger portion of the material, and the overall temperature rise is also greater. The effect of parameter τ_q is less significant compared to τ_T, in the sense that as τ_T, increases, the deviation from the Fourier model increases more rapidly.

4.3.6. Examining the Effect of Different Heat Fluxes on the Temperature Distribution of the Material

In this section, to investigate the impact of the heat flux emitted by the laser and to determine whether the non-Fourier behavior is dependent on the applied flux, the temperature of points on the material located 0.1 cm from the top of the tooth and along the axis is shown for four different heat fluxes (Figure 13).

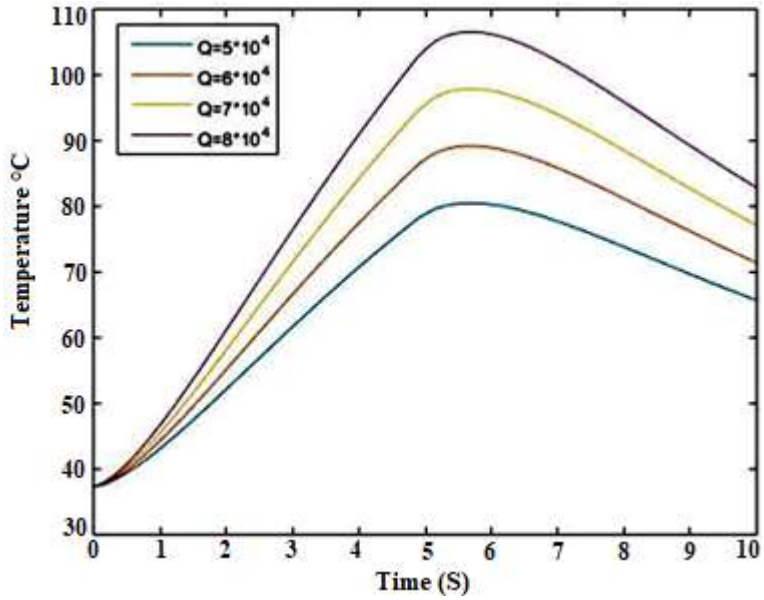

Figure 13. Investigating the effect of different fluxes on the thermal behavior of teeth in non-Fourier mode

By carefully examining Figure 11, which illustrates the temperature distribution for a fixed point under specific conditions, it can be concluded that the behavior of the non-Fourier equation is independent of temperature, and changes in temperature do not alter its overall behavior.

4. Conclusion

In this study, the distribution of tooth temperature under laser irradiation was investigated using non-Fourier equations. By solving these equations, the thermal behavior of the tooth with the assumption of limited heat transfer speed was demonstrated, and its deviation from the assumption of infinite heat transfer speed was analyzed. The results indicated that the Fourier equation unrealistically overestimates the maximum temperature attained by the material. For instance, assuming a heat flux of 2800 joules per square meter from a laser (over 5 seconds), the Fourier equation predicts a temperature difference of about 40°C, whereas experimental results report this value as approximately 22°C. If the tooth is considered as a material with non-Fourier properties with $\tau_q: 3$ & $\tau_T: 3$, the temperature difference is calculated to be around 25°C, which is closer to the experimental results. The temperature difference predicted by the Fourier and non-Fourier methods applies only to points on the tooth enamel surface and also includes internal parts of the tooth such as dentin and pulp. Many dental conditions and their treatments are related to the tooth pulp. Therefore, in laser treatments,

attention must be given to the precise temperature of these points to avoid damage to the surrounding sensitive tissues. As demonstrated, this requires considering the limited heat transfer speed (or non-Fourier methods). According to the obtained results, the tooth exhibits a completely non-Fourier behavior during laser irradiation. To accurately determine the temperature increase and thermal stresses on the tooth, it is more appropriate to use the assumption of limited heat transfer speed (non-Fourier model) rather than the assumption of infinite heat transfer speed (Fourier model). Based on the experimental work by Ms. Anna and colleagues, the appropriate parameters for the DPL method for the tooth are τ_q: 3 & τ_T: 3.

Resources

1. Lin, M., Xu, F., Lu, T. J., & Bai, B. F. (2010). A review of heat transfer in human tooth—experimental characterization and mathematical modeling. *dental materials*, *26*(6), 501-513.
2. Loganathan, S., Santhanakrishnan, S., Bathe, R., & Arunachalam, M. (2019). Prediction of femtosecond laser ablation profile on human teeth. *Lasers in Medical Science*, *34*, 693-701.
3. Kabiri, A., & Talaee, M. R. (2022). Non-Fourier bioheat model for bone grinding with application to skull base neurosurgery. *Proceedings of the Institution of Mechanical Engineers, Part H: Journal of Engineering in Medicine*, *236*(1), 84-93.
4. Kizilova, N. (2019). Bioheat equation with Fourier and non-Fourier heat transport laws: applicability to heat transfer in human tissues. *Journal of Thermal Engineering*, *5*(6), 149-161.
5. Paik, J., Kim, D., Kim, H., & Kim, H. S. (2024). Numerical analysis of thermal damage by changing irradiation angle for peri-implantitis using photothermal therapy. *Journal of Radiation Research and Applied Sciences*, *17*(4), 101054.
6. Shomalia, Z., Kovács, R., Ván, P., Kudinov, I. V., & Ghazanfariane, J. (2021). Recent progresses and future directions of lagging heat models in thermodynamics and bioheat transfer. *arXiv preprint arXiv:2103.00314*.
7. Dutta, J., Kundu, B., & Biswas, R. (2022). Analytical model for ultrashort pulse laser heating in a titanium nanofilm by implementing dual-phase-lag theory in mathematical analysis. *Journal of Thermal Analysis and Calorimetry*, 1-16.
8. Liu, K. C., & Leu, J. S. (2023). Heat transfer analysis for tissue with surface heat flux based on the non-linearized form of the three-phase-lag model. *Journal of Thermal Biology*, *112*, 103436.
9. Meena, B. S., & Kumar, S. (2024). Temperature response in skin tissue during hyperthermia based on three-phase-lag bioheat model using RBF meshfree method. *Numerical Heat Transfer, Part A: Applications*, *85*(2), 287-305.
10. Falahatkar, S., Nouri-Borujerdi, A., Mohammadzadeh, A., & Najafi, M. (2018). Evaluation of heat conduction in a laser irradiated tooth with the three-phase-lag bio-heat transfer model. Thermal Science and Engineering Progress, 7, 203-212.
11. Sabaeian, M., & Shahzadeh, M. (2015). Simulation of temperature and thermally induced stress of human tooth under CO 2 pulsed laser beams using finite element method. Lasers in medical science, 30, 645-651.
12. Chiang, Y. C., Lee, B. S., Wang, Y. L., Cheng, Y. A., Chen, Y. L., Shiau, J. S., ... & Lin, C. P. (2008). Microstructural changes of enamel, dentin–enamel junction, and dentin induced by irradiating outer enamel surfaces with CO 2 laser. Lasers in medical science, 23, 41-48.
13. Lau, X. E., Liu, X., Chua, H., Wang, W. J., Dias, M., & Choi, J. J. E. (2023). Heat generated during dental treatments affecting intrapulpal temperature: A review. Clinical Oral Investigations, 27(5), 2277-2297.
14. Wight, N. M., Acosta, E., Vijayaraghavan, R. K., McNally, P. J., Smirnov, V., & Bennett, N. S. (2017). A universal method for thermal conductivity measurements on micro-/nano-films with and without substrates using micro-Raman spectroscopy. Thermal science and engineering progress, 3, 95-101.
15. Wang, Y., Liu, J., Wang, C., Fan, X., Liu, Z., Huang, X., ... & Zhang, Y. (2024). Numerical analysis and experimental verification of time-dependent heat conduction under the action of ultra-short pulse laser. Frontiers in Physics, 12, 1416064.

16. Petersen, M., Braun, A., & Franzen, R. (2024). Thermal Effects on Dental Pulp during Laser-Assisted Bleaching Procedures with Diode Lasers in a Clinical Study. Journal of Clinical Medicine, 13(8), 2301.
17. Deppe, H., Ahrens, M., Behr, A. V., Marr, C., Sculean, A., Mela, P., & Ritschl, L. M. (2021). Thermal effect of a 445 nm diode laser on five dental implant systems: An in vitro study. Scientific reports, 11(1), 20174.
18. Tian, T., Li, C. Y., Xu, T. H., Meng, X. J., & Wu, Q. F. (2023, March). Two-dimensional heat transfer mathematical model study on multi-layers skin subjected to laser heating and air cooling. In *International Conference on Optoelectronic Materials and Devices (ICOMD 2022)* (Vol. 12600, pp. 325-332). SPIE.
19. Yakovlev, E., Shandybina, G., & Shamova, A. (2019). Modelling of the heat accumulation process during short and ultrashort pulsed laser irradiation of bone tissue. *Biomedical optics express*, *10*(6), 3030-3040.
20. Falkenstein, F., Gutknecht, N., & Franzen, R. (2014). Analysis of laser transmission and thermal effects on the inner root surface during periodontal treatment with a 940-nm diode laser in an in vitro pocket model. *Journal of Biomedical Optics*, *19*(12), 128002-128002.
21. Hibst, R., Stock, K., Gall, R., & Keller, U. (1996, December). Controlled tooth surface heating and sterilization by Er: YAG laser radiation. In *Laser applications in medicine and dentistry* (Vol. 2922, pp. 119-126). SPIE.
22. Al-Maliky, M. A., Frentzen, M., & Meister, J. (2020). Laser-assisted prevention of enamel caries: a 10-year review of the literature. *Lasers in Medical Science*, *35*, 13-30.
23. Kniha, K., Heussen, N., Weber, E., Möhlhenrich, S. C., Hölzle, F., & Modabber, A. (2020). Temperature threshold values of bone necrosis for thermo-explantation of dental implants—a systematic review on preclinical in vivo research. *Materials*, *13*(16), 3461.
24. Braun, A., Krillke, R. F., Frentzen, M., Bourauel, C., Stark, H., & Schelle, F. (2015). Heat generation caused by ablation of dental hard tissues with an ultrashort pulse laser (USPL) system. *Lasers in medical science*, *30*, 475-481.
25. Al-Karadaghi, T. S., Gutknecht, N., Jawad, H. A., Vanweersch, L., & Franzen, R. (2015). Evaluation of temperature elevation during root canal treatment with dual wavelength laser: 2780 nm Er, Cr: YSGG and 940 nm diode. *Photomedicine and laser surgery*, *33*(9), 460-466.
26. Pergolini, D., Palaia, G., De Angelis, R., Rocchetti, F., Podda, G. M., Tenore, G., ... & Romeo, U. (2023). SEM Evaluation of Thermal Effects Produced by a 445 nm Laser on Implant Surfaces. *Dentistry Journal*, *11*(6), 148.
27. Antaki, P. J. (2005). New interpretation of non-Fourier heat conduction in processed meat. *J. Heat Transfer*, *127*(2), 189-193.
28. Zhou, J., Zhang, Y., & Chen, J. K. (2009). An axisymmetric dual-phase-lag bioheat model for laser heating of living tissues. *International Journal of Thermal Sciences*, *48*(8), 1477-1485.